Cellular Oncology (2025) 48:637–654
https://doi.org/10.1007/s13402-025-01037-w

RESEARCH

UBE2Q2 promotes tumor progression and glycolysis of hepatocellular carcinoma through NF-κB/HIF1α signal pathway

Xiaoling Wu[1,2,3] · Yiran Chen[1,4] · Wenzhi He[1,5] · Ye Yao[1,5] · Yingyi Liu[1,5] · Peng Xia[1,5] · Hao Zhang[1,5] · Xiaomian Li[1,5] · Yonghua Guo[1,5] · Xi Chen[1,5] · Weijie Ma[1,5] · Yufeng Yuan[1,5]

Accepted: 8 January 2025 / Published online: 20 January 2025

Abstract

Purpose Metabolic reprogramming, particularly the Warburg effect, plays a crucial role in the onset and progression of tumors. The ubiquitin-conjugating enzyme E2 Q2 (UBE2Q2) has been identified overexpressed in hepatocellular carcinoma (HCC). Our aim was to determine if UBE2Q2 plays a role in regulating glycolysis, contributing to the carcinogenesis of HCC.

Methods Bioinformatics analysis, western blot and qPCR were used to detect the expression of UBE2Q2. Functional experiments, proteomics analysis and subcutaneous tumors were constructed to find the biological function of UBE2Q2 in HCC. Co-immunoprecipitation, western blot and ubiquitination assays were used to identify the mechanisms involved.

Results We found a significant association between high UBE2Q2 expression and poor prognosis in HCC patients. Functionally, UBE2Q2 was shown to advance tumor progression in HCC through both in vitro assays and in vivo assessments. Proteomics analysis and glycolysis stress tests corroborated an increase in glycolytic activity due to UBE2Q2. Our findings reveal that UBE2Q2 augments glycolysis by boosting the transcription levels of hypoxia-inducible factor 1α (HIF1α), primarily through the activation of the nuclear factor kappa-light-chain-enhancer of activated B cells (NF-κB) pathway. At the molecular level, UBE2Q2 interaction with baculoviral IAP repeat-containing 2 (cIAP1) orchestrates the K63-linked ubiquitination of receptor-interacting serine/threonine-protein kinase 1 (RIP1), which in turn, activates the NF-κB signaling pathway.

Xiaoling Wu and Yiran Chen contribute to this study equally.

✉ Xi Chen
chenxi2022@whu.edu.cn

✉ Weijie Ma
mawj1990@whu.edu.cn

✉ Yufeng Yuan
yuanyf1971@whu.edu.cn

Xiaoling Wu
21111210112@m.fudan.edu.cn

Yiran Chen
23111210121@m.fudan.edu.cn

Wenzhi He
hewz@whu.edu.cn

Ye Yao
yaoye2019@whu.edu.cn

Yingyi Liu
2013302180342@whu.edu.cn

Peng Xia
qazwsx1573@126.com

Hao Zhang
zhanghao617@email.sdu.edu.cn

Xiaomian Li
lixiaomian@whu.edu.cn

Yonghua Guo
yonghuaguo@whu.edu.cn

[1] Department of Hepatobiliary and Pancreatic Surgery, Zhongnan Hospital of Wuhan University, 169 Donghu Road, Wuhan, Hubei 430071, PR China

[2] Department of Liver Surgery, Key Laboratory of Carcinogenesis and Cancer Invasion of Ministry of Education, Zhongshan Hospital, Liver Cancer Institute, Fudan University, Shanghai, China

[3] Research Unit of Liver Cancer Recurrence and Metastasis, Chinese Academy of Medical Sciences, Beijing, China

[4] Key Laboratory of Carcinogenesis and Cancer Invasion of Ministry of Education, Shanghai, China

[5] Clinical Medicine Research Center for Minimally Invasive Procedure of Hepatobiliary & Pancreatic Diseases of Hubei Province, Wuhan, Hubei 430071, PR China

Conclusions Our investigation reveals that UBE2Q2 regulates the glycolysis in HCC through modulation of the NF-κB/HIF1α signaling pathway, pinpointing UBE2Q2 as a promising therapeutic target for the disease.

Graphical abstract

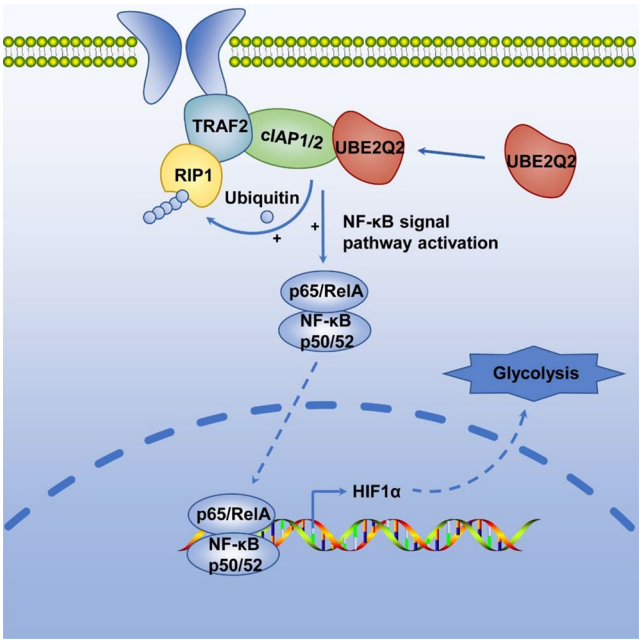

Keywords Hepatocellular carcinoma · UBE2Q2 · HIF1α · NF-κB signaling pathway · Ubiquitination

Abbreviations

AFP	Alpha-fetoprotein
CCK-8	Cell Counting Kit-8
BCLC	Barcelona Clinic Liver Cancer
cIAP1	Baculoviral IAP repeat containing 2
CHX	Chlorhexidine
Co-IP	Co-immunoprecipitation
ECAR	Extracellular acidification rate
HIF1α	Hypoxia-inducible factor 1α
GSEA	Gene Set Enrichment Analysis
HCC	Hepatocellular carcinoma
IF	Immunofluorescence
IHC	Immunohistochemical staining
KEGG	Kyoto Encyclopedia of Genes and Genomes
MS	Mass spectrometry
NCBI	National Center for Biotechnology Information
NF-κB	Nuclear factor kappa B
qRT-PCR	Quantitative real-time PCR
RIP1	Receptor interacting serine kinase 1
siRNA	Small interfering RNA
TCGA	The Cancer Genome Atlas
TGFβ	Transforming growth factorβ
TRAF2	TNF receptor associated factor 2
UBC	Ubiquitin conjugation
UBE2Q2	Ubiquitin conjugating enzyme E2 Q2
VEGF	Vascular endothelial growth factor
WB	Western Blot

1 Introduction

Primary liver cancer is one of the most common malignant tumors in the world [1]. The main pathological type of primary liver cancer is hepatocellular carcinoma (HCC), accounting for over 80% of the total cases [2]. The difficulty of early diagnosis contributes to high proportion of advanced-stage HCC cases [3]. At present, targeted drugs like Sorafenib and Lenvatinib have become the first-line treatment for advanced HCC. However, the complex pathogenesis of HCC results in limited efficacy with single targeted drug [4]. Therefore, it is necessary to search for new targets to further explore the mechanism of tumor progression and broaden selection of therapeutic drugs for HCC.

Tumor cells possess a unique metabolic feature, named "Warburg effect", which result in increased level of glycolysis and more production of lactate [5]. Various studies have

confirmed that glycolysis plays a crucial part in the growth of different types of tumors, including HCC [6–8]. The Warburg effect facilitates adaptation of hepatocellular carcinoma (HCC) cells to hypoxic and low-oxygen environments [9]. Meanwhile, the hypoxic environment inside usually leads to the increased expression of hypoxia-inducible factors in tumor cells [10]. Among them, Hypoxia-inducible factor 1α (HIF1α) is a well-studied transcription factor subunit which could regulate over 100 downstream genes required for glycolysis and tumor progression [11]. Recent studies have reported that several signaling pathways, including Wingless/Integrated (WNT) pathway, Mitogen-activated protein kinase (MAPK) pathway, Phosphatidylinositol-3-Kinase/Protein Kinase B/Mammalian Target of Rapamycin (PI3K/AKT/mTOR) pathway, Nuclear Factor kappa-light-chain-enhancer of activated B cells (NF-κB) pathway etc. could regulate the transcriptional of HIF1α [12–16]. Besides, proline residue hydroxylation leads to the degradation of HIF1α regulated by von Hippel-Lindau tumor suppressor (pVHL) E3 ligase complex [17]. However, there are still some molecules that affect HIF1α and cellular glycolysis waiting to be discovered.

Ubiquitination which mainly depends on ubiquitin, ubiquitin-activating enzyme (E1), ubiquitin-conjugating enzyme (E2) and ubiquitin ligase (E3) could regulate protein stability, activation of related signaling pathways and gene transcription [18]. Ubiquitin conjugating enzyme E2 Q2 (UBE2Q2) contains a conserved ubiquitin conjugation (UBC) domain at its C-terminal, which can directly bind with ubiquitin, suggesting that it might play a role of ubiquitin conjugating enzyme to determine the ubiquitination modification type of the substrate protein and affect biological functions of the substrate protein [19]. Researchers have demonstrated that UBE2Q2 is abnormally overexpressed in hypopharyngeal tumors and pediatric acute lymphoblastic leukemia [20, 21]. In HeLa cells, UBE2Q2 antagonizes early mitotic checkpoints. The interference of UBE2Q2 may increase the sensitivity of tumor cells to chemotherapy drugs [19]. However, there is no detailed research on the biological function of UBE2Q2 in HCC, or its role in the process of protein ubiquitination.

In this study, we found that UBE2Q2 promoted the progression of HCC. Besides, we discovered that UBE2Q2 could play a new role in NF-κB signaling pathway and regulate glycolysis of HCC. In consideration of the close association between glycolysis and tumorigenesis, this study provided a potential therapeutic target for HCC.

2 Materials and methods

2.1 Clinical HCC patients' samples and information

Tumor and adjacent normal liver tissues of 80 HCC patients (68 male and 12 female patients) on whom the liver resections were performed during 2018 to 2020 in the Department of Hepatobiliary and Pancreatic Surgery, Zhongnan Hospital of Wuhan University were collected. None of the patients received any pre-operative therapy like radiofrequency ablation, anhydrous alcohol injection, TACE or immunotherapy. The histopathological examination of samples was confirmed by two experienced pathologists. Related clinical data of 80 patients were recorded for statistical analysis.

2.2 Cell culture

The cell lines Huh-7, HCC-LM3, Hep3B, HepG2, HepG2.2.15, and SK-Hep-1 were obtained from the Shanghai Cell Bank of the Chinese Academy of Medical Sciences. These were cultured under standard conditions: Dulbecco's Modified Eagle Medium (DMEM) supplemented with 10% fetal bovine serum and 1% penicillin/streptomycin, maintaining a temperature of 37 °C and a 5% CO_2 atmosphere. Cell line authenticity was verified through STR profiling and all were certified mycoplasma-free.

For specific experiments, Huh-7 and LM3 cell lines underwent treatment with distinct agents: 100 μM cobalt chloride for 12 h; 10 μM chlorhexidine, corynoxeine, or LY294002, each for a period of 24 h; 20 μM rapamycin for 24 h; 20 μM (-)-DHMEQ for 24 h and 2 mM 2-DG for 12 h. All aforementioned compounds were sourced from Sigma Aldrich (Germany) and MCE (USA).

2.3 RNA extraction, reverse transcription, and quantitative real-time PCR (qRT-PCR)

RNA from both tissue specimens and cultured cells was isolated using TRIzol Reagent (Invitrogen, USA). The quality and concentration of RNA were assessed with a NanoDrop ND2000 spectrophotometer (Thermo Scientific, Massachusetts, USA). Reverse transcription was conducted using the HiScript III 1st Strand cDNA Synthesis Kit for mRNA and the Mir-X miRNA First-Strand Synthesis Kit (Takara, USA), following the provided protocols. Quantitative real-time PCR was performed with a SYBR Green PCR kit (Vazyme, China) on a CFX96TM Real-time PCR Detection System (Bio-Rad, California, USA). Relative RNA expression levels were quantified using the 2^(-ΔΔCt) method, with the threshold cycle (Ct) being determined. Reproducibility was ensured by conducting all procedures

in triplicate. Primer sequences used are detailed in Table S1 of the supplementary materials.

2.4 RNA interference and cell transfection

UBE2Q2 expression was targeted for knockdown using small interfering RNAs (siRNAs). Three distinct siRNAs aimed at UBE2Q2 (referred to as siRNA #1, siRNA #2, and siRNA #3) were custom-synthesized by Genecreate (Wuhan, China). Among them, siRNA #2 was subsequently labeled as siUBE2Q2 in Figs. 4 and 5 and Fig. S4. The details of these siRNA and shRNA sequences are provided in Table S2 of the supplementary materials. For the siRNA transfection, the Genmute transfection reagent (Signagen, Maryland, USA) was used, following the manufacturer's protocol.

2.5 Construction of plasmid, lentivirus package and cell infection

The UBE2Q2 gene was synthesized and cloned into the pEZ-Lv105 vector to create an overexpression construct, hereafter referred to as UBE2Q2 plasmid. The empty pEZ-Lv105 vector was utilized as a control, designated as Vector. Both plasmids were products of GeneCopoeia (Rockville, USA). Additional plasmids, including pcDNA-HA-UBE2Q2, pcDNA-HIF1α, pcDNA-His-TRAF2, and pcDNA-Flag-cIAP1, were synthesized by Genecreate (Wuhan, China). Plasmids pCDEF-HA-Ub(K11), pCDEF-HA-Ub(K48), and pCDEF-HA-Ub(K63) were procured from Ke Lei Biological Technology (Shanghai, China). Transfections were carried out using Lipofectamine 3000 (Thermo Fisher Scientific, CA, USA) according to the manufacturer's recommendations.

Stable UBE2Q2 knockdown and overexpression lines were established using lentiviral systems (Lv-shUBE2Q2 and UBE2Q2 respectively), also provided by Genecreate (Wuhan, China), with a virus titer of 6×10^8 TU/mL. For infection, a multiplicity of infection (MOI) of 10 was applied to Huh-7 cells, with 100 µL of viral suspension coupled with 100 µL of Hitrans P virus infection reagent (GeneChem, Shanghai, China) per 1×10^6 cells. After 24 h, the medium was replenished. Cells were collected 4 days post-infection and selected with puromycin. The knockdown efficiency was evaluated using qRT-PCR and Western blot analyses.

2.6 Cell viability assays

Cell viability was assessed using the Cell Counting Kit-8 (CCK-8, Biosharp, China) assay. Briefly, cells were seeded at a density of 5,000 per well in 100 µL of culture medium in a 96-well plate. Afterward, 10 µL of CCK-8 solution was added to each well. The plate was incubated at 37 °C for 1 h before measuring the absorbance at 450 nm using a microplate reader.

2.7 Colony formation assays

A colony formation assay was performed by plating 500 to 1,000 cells in a six-well plate and culturing for 14 days. The colonies were then fixed with 4% paraformaldehyde and stained for 1 h with 0.1% crystal violet (Sigma Aldrich, Germany). Post-staining, colonies were counted and imaged using a stereomicroscope.

2.8 Wound healing assay

Cell transfection and culture were performed in a six-well plate. Upon reaching confluence, a 100 µL pipette tip was used to create a straight scratch through the cell monolayer. Subsequently, cells were incubated in serum-free DMEM. Wound closure was documented at 0 h, 24 h and 48 h post-scratch, and analyzed using Image J software.

2.9 Cell invasion and migration assays

Migration and invasion assays were conducted using a 24-well plate with a Transwell insert (8 µm pore size, BD Biosciences, USA). Medium with 10% FBS (600 µL) was added to the lower chamber. For invasion assays, the upper insert was precoated evenly with Matrigel (Sigma Aldrich, Germany). Subsequently, 1×10^4 cells in 200 µL of serum-free medium were seeded into the upper chamber. Following a 48 h incubation period, non-invading or non-migratory cells were removed. Cells were fixed with 4% paraformaldehyde for 30 min and then stained with 0.1% crystal violet (Sigma Aldrich, Germany) for 1 h. After washed by sterile water, cells were observed using an inverted fluorescence microscope (Olympus, Japan). Results were examined and documented in three random fields of view.

2.10 Detection of cell cycle and apoptosis

Cell cycle and apoptosis analyses were performed utilizing the Annexin V FITC/PI Apoptosis and Cell Cycle Kit (MultiSciences, China) following the manufacturer's protocol. Flow cytometric analysis was performed using a Beckman instrument (USA).

2.11 In vivo experiments

Four-week-old male athymic BALB/C-nude mice were acquired from SPF Biotechnology (Beijing, China). All

experimental procedures and husbandry were conducted at the Center for Animal Experiment at Wuhan University. The mice were randomly assigned and identified in two groups, with five mice per group, for the establishment of a subcutaneous tumor model. A stable UBE2Q2 knockdown cell line (Lv-shUBE2Q2) was generated using Huh-7 cells. For tumor induction, 5×10^6 cells were injected subcutaneously into the right axillary region of each mouse. Commencing on day 7 post-inoculation, mice received 100 mg/kg of PX-478 in PBS by intraperitoneal injection bi-daily. Tumor sizes were measured tri-weekly. After 3–4 weeks, the mice were euthanized, tumors were excised, and preserved in formalin for further immunohistochemical analysis.

2.12 HE and immunohistochemical staining (IHC)

Tissues intended for hematoxylin and eosin (H&E) or immunohistochemical (IHC) staining were fixed in 4% paraformaldehyde solution. These were then dehydrated, embedded in paraffin, and sectioned to produce tissue slices. Then each section was stained with H&E or with primary antibody such as UBE2Q2 antibody, HIF1α antibody or Ki67 antibody etc. Detailed information of primary antibodies used in IHC is provided in **Table S3** of the supplementary materials. Imaging was conducted using an Aperio VERSA 8 automatic digital scanning and analysis system (Leica Biosystems, Germany), and the images were quantitatively analyzed with Aperio ImageScope software.

2.13 Proteomics assay

The HCC-LM3 cells transfected with UBE2Q2 plasmids constituted the experimental group, while those transfected with empty vector plasmids served as the control. Cells were harvested 48 h post-transfection. Cell pellets were lysed using a protein lysis buffer containing 7 M urea, 2 M thiourea, 4% SDS, 40 mM Tris-HCl (pH 8.5), 1 mM PMSF, and 2 mM EDTA. The lysate was sonicated for 15 min, then centrifuged at 4 °C for 20 min to collect the protein precipitate. The resulting samples were submitted in triplicate for proteomic analysis at Singleronbio (Nanjing, China). Peptides were tagged using the iTRAQ-8 kit (SCIEX), and peptide detection was conducted with TripleTOF 5600plus mass spectrometry. ProteinPilot V4.5 software was utilized for protein identification and quantification. Differential protein expression was determined based on fold change and P-value; proteins exhibiting a fold change of ≥ 1.5 (upregulated) or ≤ 0.67 (downregulated) with a P-value of ≤ 0.05 were considered significant.

2.14 Co-immunoprecipitation (Co-IP) and mass spectrometry (MS)

Huh-7 cells were grown in 10 cm diameter culture dishes and co-transfected with various plasmids for subsequent co-immunoprecipitation experiments. The cells were harvested and placed into 2 mL centrifuge tubes. Each tube was treated with 1 mL of IP buffer (comprising 20 mM Tris-HCl (pH 7.4), 150 mM NaCl, 1 mM EDTA (pH 8.0), 1% NP-40, and 1×Protease and Phosphatase Inhibitor Cocktail) to lyse the cells for 30 min. Pre-washed Protein A/G Magnetic beads from MCE (USA) were introduced into the tubes and the mixture was agitated on a disc rotator mixer for another 30 min. Target-specific antibodies were then added to the respective tubes and incubated for over 3 h at 4 °C. After the incubation, beads were collected by centrifugation at 5,000 rpm for 2 min at 4 °C and washed 4 times with ice-cold wash buffer (10 mM Tris/Cl pH 7.5, 150 mM NaCl, 0.5 mM EDTA). The beads were resuspended with 40 µl of 2× sample buffer and boiled for 3 min. Immunoprecipitates were separated by SDS-PAGE and sent for mass spectrometry analysis (Hangzhou Cosmos Wisdom Biotechnology).

2.15 Western blot (WB)

Tissue and cellular proteins were extracted using RIPA lysis buffer supplemented with 1×PMSF proteasome inhibitor, both sourced from Beyotime (China). Protein concentrations were quantified using a BCA assay kit provided by Thermo Fisher Scientific (CA, USA). Proteins were resolved by electrophoresis on 7-10% SDS-PAGE gels and subsequently transferred onto polyvinylidene fluoride (PVDF) membranes. The membranes were blocked with 5% non-fat milk for 1 h before overnight incubation at 4°C with primary antibodies. Following a series of washes, the membranes were incubated with the corresponding secondary antibodies for 90 min at room temperature. Then membranes were dipped in ECL Substrate Luminol solution from Bio-Rad (CA, USA). Chemiluminescence detection was performed using the Tanon-5200 imager (Shanghai, China). Comprehensive antibody details were included in **Table S3** of the supplementary materials.

2.16 Glucose uptake and lactate production

Designated cells were transfected with UBE2Q2 plasmids, HIF1α plasmids, empty vector plasmids, siUBE2Q2, and siRNA NC in line with the experimental protocol, and then seeded into 96-well plates. At the 24 h mark, glucose uptake and lactate secretion were quantified using the Glucose Uptake Colorimetric Assay Kit and the L-Lactate Assay Kit, respectively, both from Sigma Aldrich (Germany) and

in strict accordance with the provided manufacturer's protocols. Absorbance readings at 412 nm were captured using an enzyme-linked immunosorbent assay reader.

2.17 Immunofluorescence (IF)

Huh-7 and HCC-LM3 cells fixed in 4% paraformaldehyde were permeabilized using 0.5% Triton X-100 for 15 min. Subsequently, cells were blocked with 5% bovine serum albumin (BSA) for 1 h at room temperature before overnight primary antibody incubation at 4 °C. After thorough washing with PBS, the cells were incubated with fluorescently labeled secondary antibodies for 1 h at room temperature within a humidified chamber. Following this, cells were mounted with DAPI to stain nuclei and visualized with an Olympus FluoView™ FV1000 confocal microscope.

2.18 Seahorse bioanalyzer

Cells transfected with the appropriate plasmids or siRNA were plated at a density of 4×10^4 cells per well in XF24 microplates (Seahorse Agilent, USA). The assay cartridge was hydrated in a CO_2-free incubator at 37 °C overnight. The next day, cells were switched to a specialized assay medium before the extracellular acidification rate (ECAR) or oxygen consumption rate (OCR) was measured using a Seahorse XF24 Analyzer's sensor probe, adhering to the manufacturer's guidelines. For ECAR, glycolysis stress tests were conducted with Seahorse XF cell glycolysis stress test kits, and the data were processed using Wave software. For OCR, oxygen consumption tests were conducted with Seahorse XF cell mito stress test kits, and the data were processed using Wave software.

2.19 In vivo ubiquitination assays

Following 48 h post-transfection, Huh-7 cells transfected with pEZ-UBE2Q2 or vector plasmids and treated with cobalt chloride were harvested. Additionally, Huh-7 cells co-transfected with pEZ-UBE2Q2 and mutant ubiquitin plasmids—pCDEF-HA-Ub(K11) (all lysine was mutant to arginine except from wild-type lysine 11), pCDEF-HA-Ub(K48) (all lysine was mutant to arginine except from wild-type lysine 48), or pCDEF-HA-Ub(K63) (all lysine was mutant to arginine except from wild-type lysine 63)—were collected after 48 h. Cell pellets from each group were lysed in IP lysis buffer. Subsequent procedures were coherent with those previously described for co-immunoprecipitation (Co-IP).

2.20 Bioinformatics analysis

UBE2Q2 expression in paired tissue samples and associated Kaplan-Meier survival curves for hepatocellular carcinoma (HCC) patients were extracted from The Cancer Genome Atlas (TCGA) database. Additional analyses of overall survival curves and correlations with UBE2Q2 in HCC were conducted using the GEPIA platform (http://gepia.cancer-pku.cn). The data for single-gene enrichment analysis were sourced from the Gene Set Enrichment Analysis (GSEA) website (http://www.gsea-msigdb.org/gsea/index.jsp), with the analysis performed using GSEA-3.0 software.

2.21 Statistical analysis

Statistical analysis was conducted using GraphPad Prism version 8.0 (GraphPad Software) and SPSS version 22.0 (SPSS, USA). Data are expressed as mean ± standard deviation (SD). The Student's t-test and non-parametric test were utilized for comparing differences between two groups, while two-way ANOVA was employed for analyses involving more than two groups. Correlations between UBE2Q2 expression and clinical parameters were determined using the chi-squared ($\chi 2$) test, with two-tailed P values. Significance levels for all tests were set as follows: $*p<0.05$, $**p<0.01$, $***p<0.001$, $****p<0.0001$, with ns denoting 'not significant'.

3 Results

3.1 UBE2Q2 is overexpressed in HCC and indicates poor prognosis of HCC patients

The expression levels of UBE2Q2 were evaluated in 80 paired tissue specimens utilizing quantitative real-time PCR (qRT-PCR). The analyses revealed a notable overexpression of UBE2Q2 in hepatocellular carcinoma (HCC) tissues compared with adjacent non-cancerous tissues (Fig. 1a), a finding that was further supported by data from The Cancer Genome Atlas (TCGA) (Fig. 1b). Furthermore, elevated UBE2Q2 expression was found to be significantly associated with decreased overall survival (OS) and disease-free survival (DFS) rates in HCC patients (Fig. 1c and d). Protein expression analyses through Western blotting (WB) and immunohistochemistry (IHC) consistently demonstrated a substantial increase in UBE2Q2 levels in HCC samples (Fig. 1e and g). The overexpression of UBE2Q2 was also prominently observed in HepG2, Hep3B, and Huh-7 cell lines when contrasted with LM3 and SK-Hep-1 cell lines, as evidenced by qRT-PCR and WB data (Fig. 1f). Immunofluorescence staining showed that UBE2Q2 primarily

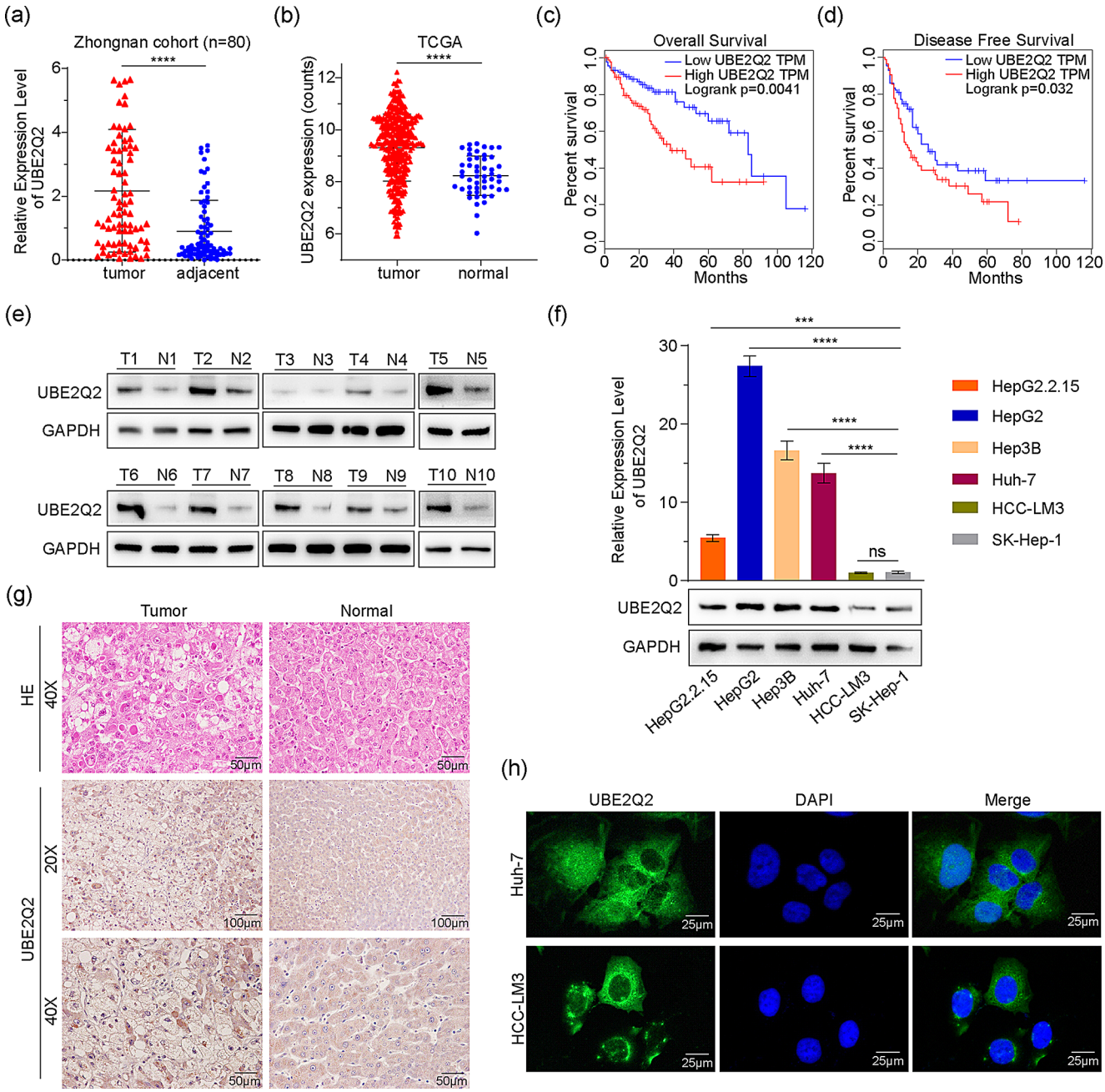

Fig. 1 UBE2Q2 overexpresses in HCC and indicates poor prognosis. (**a**) Expression level of UBE2Q2 mRNA in HCC and adjacent normal tissues from 80 clinical samples. (**b**) UBE2Q2 mRNA levels in tumor and normal tissues from GEPIA website. (Data from TCGA databases) (**c**) Kaplan-Meier OS curve of UBE2Q2 from GEPIA website. (Data from TCGA databases. Quartile expression of UBE2Q2 is used for the cutoff of groups. Log-rank test is used to calculate P value) (**d**) Kaplan-Meier DFS curve of UBE2Q2 from GEPIA website. (Data from TCGA databases. Quartile expression of UBE2Q2 is used for the cutoff of groups. Log-rank test is used to calculate P value) (**e**) WB of UBE2Q2 in 10 pairs of clinical samples. T-tumor, N-normal. (**f**) Protein expression level and mRNA level of UBE2Q2 in HCC cell lines. (**g**) HE staining and IHC staining of UBE2Q2 in tumor tissue and normal liver tissue. (**h**) Immunofluorescent staining of UBE2Q2 in Huh-7 and HCC-LM3. Data are presented as the mean ± SD. *$p<0.05$, **$p<0.01$, *** $p<0.001$. **** $p<0.0001$. LIHC, Liver hepatocellular carcinoma, ns nonsignificant difference

localizes to the cytoplasm (Fig. 1h). Additionally, high UBE2Q2 expression was significantly correlated with key clinical parameters, including increased tumor size ($p=0.010$), higher Barcelona Clinic Liver Cancer (BCLC) stage ($p=0.003$), and the presence of hepatocirrhosis ($p=0.005$) (Table 1).

3.2 UBE2Q2 facilitates the tumorigenesis of HCC in vitro and in vivo

To investigate the biological role of UBE2Q2 in hepatocellular carcinoma (HCC) cells, siRNA was employed to effectively silence the gene in Huh-7 and Hep3B cell lines. We selected siRNA #1 and siRNA #2 for subsequent experiments after the detection of gene knockdown efficacy verified through quantitative real-time PCR (qRT-PCR) and WB analysis (Fig. 2a and b). Wound healing assays indicated that UBE2Q2 suppression hindered the repair and migratory abilities of these cells (Fig. 2c). Proliferative capacities were significantly reduced as evidenced by CCK-8 and colony formation assays (Fig. 2d and e).

Conversely, UBE2Q2 expression was enhanced in HCC-LM3 and Huh-7 cells through transfection with a UBE2Q2-expressing plasmid, and the success of this overexpression was confirmed (Fig. S1a, Fig. S1c). This overexpression of UBE2Q2 was associated with increased cell proliferation (Fig. S1d, Fig. S1f). Furthermore, migration and invasion assays showed that knockdown of UBE2Q2 led to the decreased migratory and invasive potential of Huh-7 and Hep3B cells (Fig. S2a) while overexpression of UBE2Q2 enhanced migratory and invasive capacity of Huh-7 and LM3 cells (Fig. S2b).

Furthermore, UBE2Q2 knockdown led to cell cycle arrest, particularly at the G2/M transition, and increased apoptotic rates in HCC cells (Fig. 3a, c). On the other hand, overexpression of UBE2Q2 produced antithetical outcomes (Fig. 3b, d).

For in vivo analysis, a subcutaneous tumor model was generated using Huh-7 cells transduced with lenti-virus carrying shUBE2Q2 or shControl vectors (Fig. 4a), where the silencing efficiency was quantified employing qRT-PCR and WB (Fig. S1b, Fig. S1c). The volume and weight of the tumors from animals inoculated with UBE2Q2-knockdown cells were significantly lower, demonstrating a substantial inhibition of HCC cell proliferation in vivo (Fig. 4b and c), and IHC analyses showed decreased expression of the proliferation marker Ki-67 in the tumors with UBE2Q2 knockdown (Fig. 4d).

3.3 UBE2Q2 promotes the glycolysis of HCC

To determine the impact of UBE2Q2 on HCC, a proteomics analysis was performed, revealing 209 upregulated proteins and 153 downregulated proteins in the UBE2Q2 overexpression group (Fig. 4e). Notably, several upregulated proteins were implicated in glycolysis, including PKM2, PFKL, LDHA, and GLUT1 (Fig. 4e). Enrichment analysis utilizing the Kyoto Encyclopedia of Genes and Genomes (KEGG) dataset corroborated that the Glycolysis/Gluconeogenesis pathway was among those enriched (Fig. S3a). This finding aligns with results from the Gene Set Enrichment Analysis (GSEA) of single gene expressions from the TCGA Liver Cancer RNA-seq data, where gene sets associated with glycolysis were predominantly upregulated in tumor tissues with high UBE2Q2 expression (Fig. S3b). These results led to the hypothesis that UBE2Q2 could play a role in modulating glycolytic processes in HCC. Assays for glucose uptake and lactate secretion confirmed that UBE2Q2 knockdown attenuated glycolysis in HCC cells, while its overexpression had the opposite effect (Fig. 4f and g, Fig. S3c, Fig. S3d).

Table 1 Relationship between expression of UBE2Q2 and clinicopathologic features of HCC patients ($n=80$)

Clinical pathologic characteristics	*n*	UBE2Q2		*p* value
		High (%)	Low (%)	
Gender				
Male	68	37(54.4)	31(45.6)	0.060
Female	12	3(25.0)	9(75.0)	
Age (years)				
<60	47	20(42.6)	27(57.4)	0.112
≥60	33	20(60.6)	13(39.4)	
Tumor Size (cm)				
<5	60	25(41.7)	35(58.3)	0.010*
≥5	20	15(75)	5(25)	
Tumor Number				
Singular	69	37(53.6)	32(46.4)	0.105
Multifocal	11	3(27.3)	8(72.7)	
PVTT				
Yes	12	7(58.3)	5(41.7)	0.531
No	68	33(48.5)	35(51.5)	
TNM Stage				
Stage I - II	66	30(45.5)	36(54.5)	0.077
Stage III-IV	14	10(71.4)	4(28.6)	
BCLC Stage				
A	56	22(39.3)	34(60.7)	0.003*
B-C	24	18(75)	6(25)	
AFP (ng/L)				
≤400	47	21(44.7)	26(53.3)	0.256
>400	33	19(57.6)	14(42.4)	
HBV infection				
Yes	58	31(53.4)	27(46.6)	0.317
No	22	9(40.1)	13(59.9)	
Hepatocirrhosis				
Yes	59	35(59.3)	24(40.7)	0.005*
No	21	5(23.8)	16(76.2)	

Abbreviation: AFP, alpha fetoprotein; BCLC, Barcelona Clinic Liver Cancer; HBV, Hepatitis B virus; PVTT, portal vein tumor thrombus.
* $p<0.05$

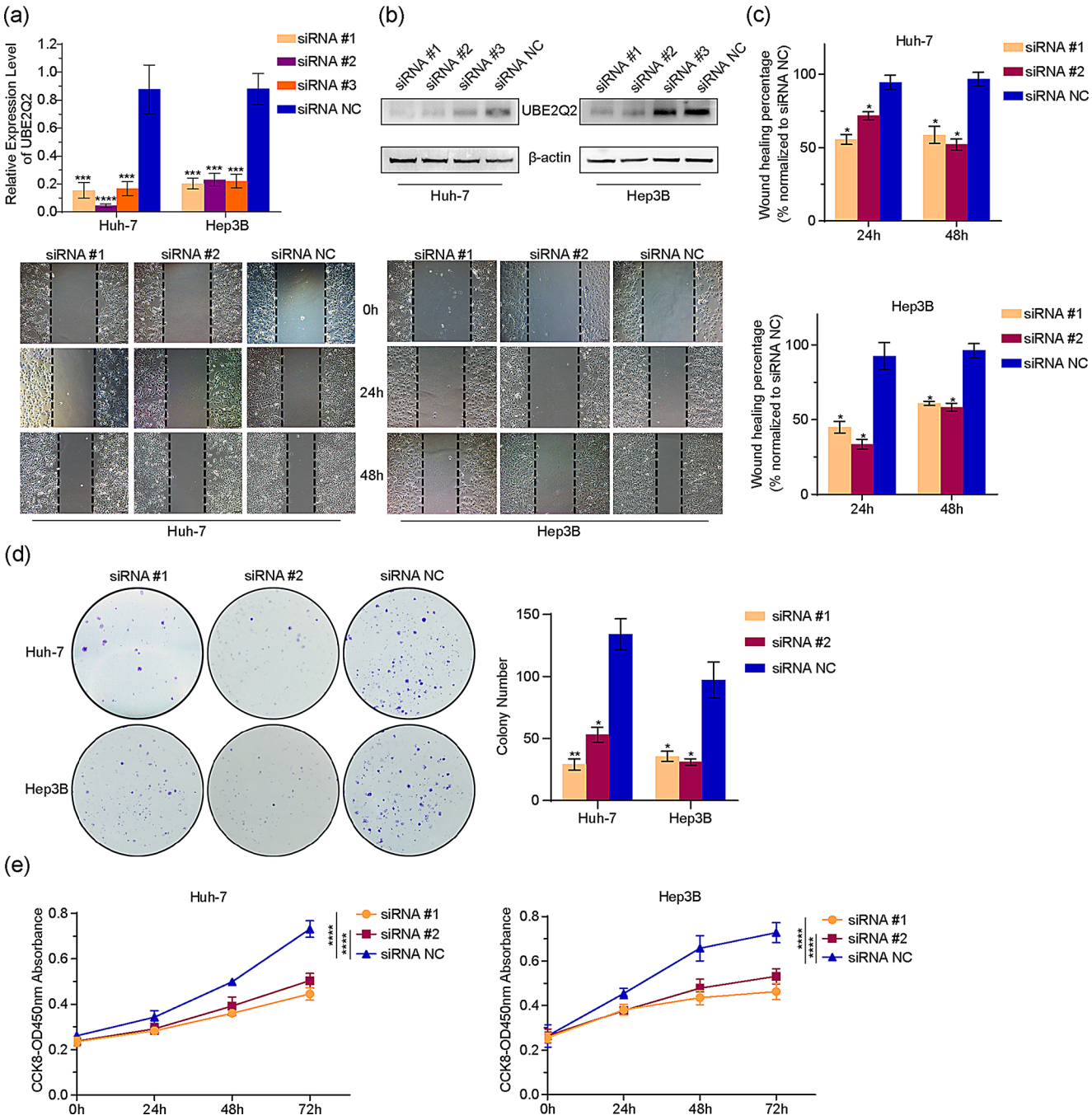

Fig. 2 Knockdown of UBE2Q2 represses the proliferation and migration ability of HCC cells in vitro. (**a**) The interference efficiency of siRNA measured by qRT-PCR. (**b**) The interference efficiency of siRNA measured by WB. (**c**) Wound healing assay of Huh-7 and Hep3B transfected by siRNA1, siRNA2 and siRNA NC. (**d**) Colony assay of Huh-7 and Hep3B transfected by siRNA1, siRNA2 and siRNA NC. (**e**) CCK-8 assay of Huh-7 and Hep3B transfected by siRNA1, siRNA2 and siRNA NC. Data are presented as the mean ± SD. *$p<0.05$, **$p<0.01$, ***$p<0.001$, ****$p<0.0001$

Moreover, energetic metabolism assessment through extracellular acidification rate (ECAR) and oxygen consumption rate (OCR) measurements showed that UBE2Q2 elevated glycolytic function and mitochondrial respiration capacity in Huh-7 cells (Fig. 4h, Fig. S3e, Fig. S3f). CCK-8 suggested that inhibition of glycolysis using 2-DG could block the proliferative effect of UBE2Q2 overexpression on HCC cells (Fig. S3g). The use of 2-DG effectively blocked the increase of lactate secretion and migration capacity in HCC cells caused by UBE2Q2 overexpression (Fig. S3h, Fig. S3i).

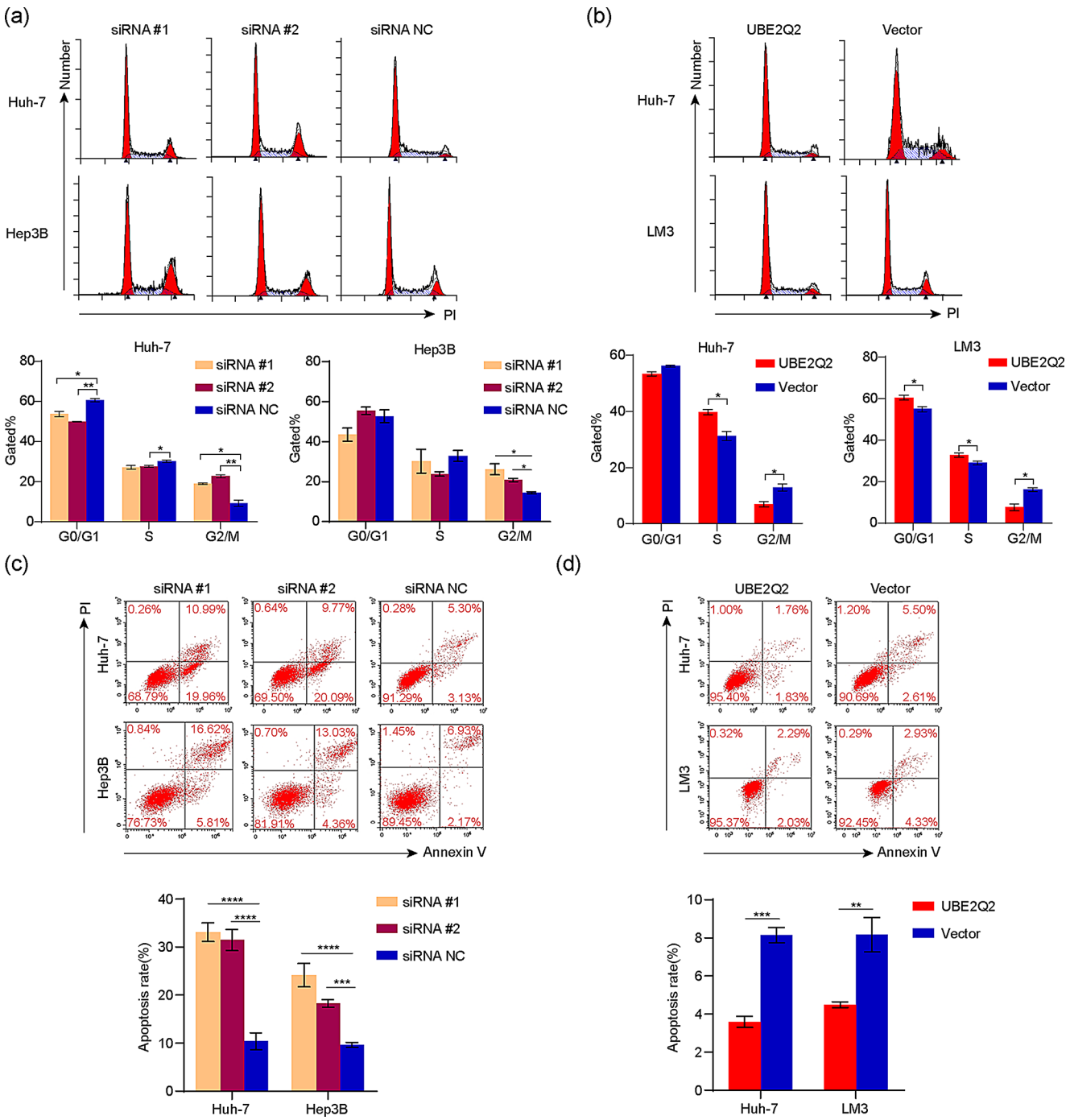

Fig. 3 Abnormal expression of UBE2Q2 affects cell cycle distribution and apoptosis rate of HCC cells. (**a**) Cell cycle distribution of Huh-7 and Hep3B transfected by siRNA1, siRNA2 and siRNA NC. (**b**) Cell cycle distribution of Huh-7 and LM3 transfected by UBE2Q2 and empty vector plasmids. (**c**) Apoptosis rate of Huh-7 and Hep3B transfected by siRNA1, siRNA2 and siRNA NC. (**d**) Apoptosis rate of Huh-7 and LM3 transfected by UBE2Q2 and empty vector plasmids. Data are presented as the mean±SD. *$p<0.05$, **$p<0.01$, ***$p<0.001$, ****$p<0.0001$

3.4 UBE2Q2 promotes HCC glycolysis by enhancing the transcription level of HIF1α

Delving deeper into the mechanism by which UBE2Q2 enhances glycolysis in HCC, we observed an upregulation of HIF1α in the UBE2Q2 overexpression cohort. The KEGG pathway enrichment analysis of our proteomic data also implicated the HIF1 signaling pathway (Fig. S3a). Building upon existing literature where HIF1α elevation was shown to activate glycolysis via induction of glycolytic

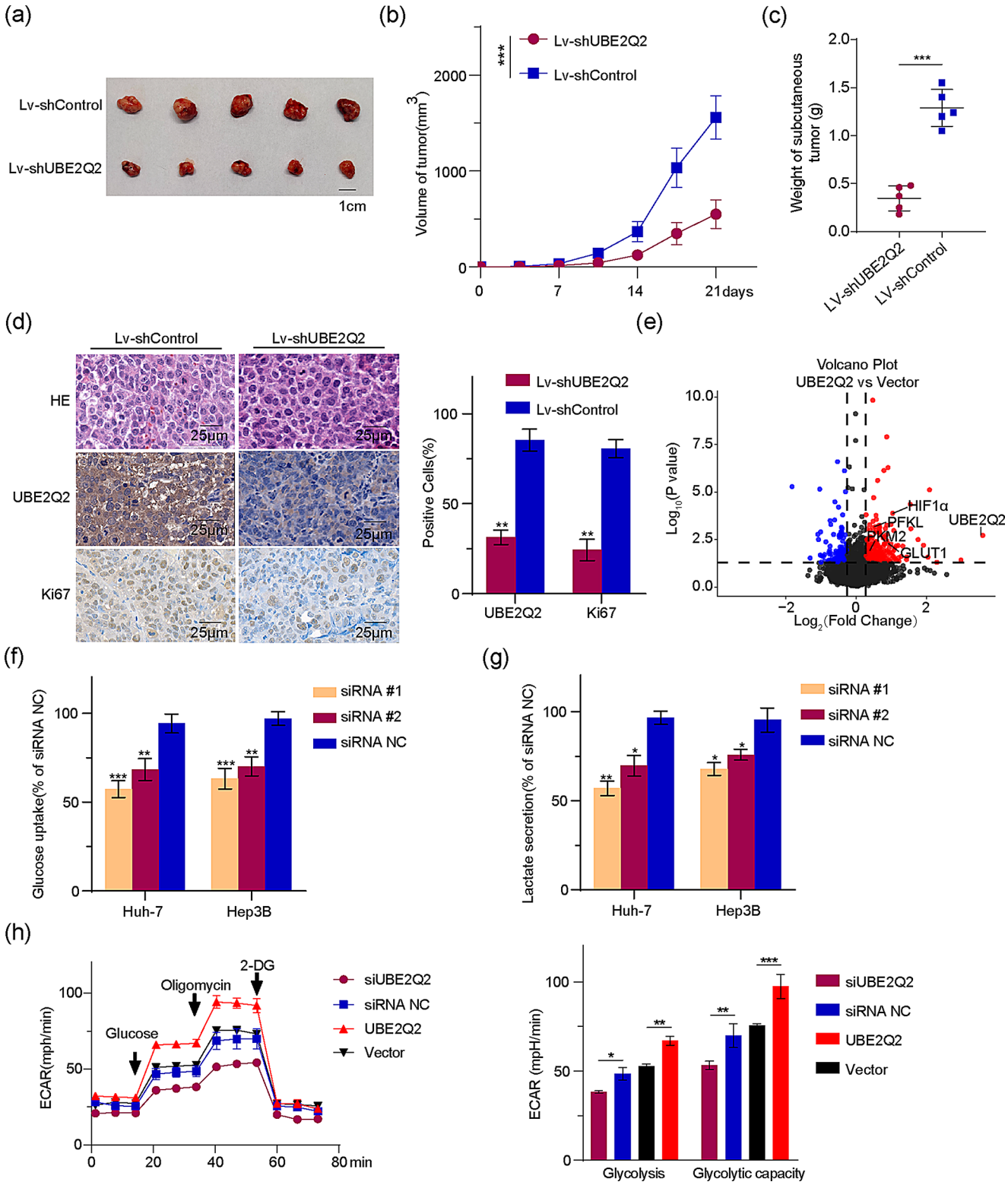

Fig. 4 UBE2Q2 facilitates the tumorigenesis in vivo and promotes glycolysis in HCC. (**a**) The construction of subcutaneous tumor model by Huh-7 infected by Lentivirus-shUBE2Q2 or Lentivirus-shControl. (**b**) The growth curve of subcutaneous tumors. (**c**) The weight of subcutaneous tumors. (**d**) Representative HE staining and IHC staining images of subcutaneous tumors and quantification. (**e**) Volcano Plot of proteomics assay from LM3 cells transfected with UBE2Q2 plasmid compared with empty vector plasmid. The blue dots represent down-regulated proteins and red dots represent up-regulated proteins. (**f**) Glucose uptake of Huh-7 and Hep3B transfected by siRNA1, siRNA2 and siRNA NC. (**g**) Lactate secretion assay of Huh-7 and Hep3B transfected by siRNA1, siRNA2 and siRNA NC. (**h**) Extracellular acidification rate detected from Huh-7 cells transfected by siRNA and plasmids. Data are presented as the mean ± SD. *$p<0.05$, **$p<0.01$, ***$p<0.001$. ECAR, Extracellular acidification rate

enzymes and GLUTs [22, 23], and given our prior findings of similar protein upregulations, we surmised that UBE2Q2 overexpression would heighten HIF1α levels. IHC staining in subcutaneous tumors also demonstrated that the expression levels of glycolytic proteins such as PFKL, PKM2, GLUT1, LDHA and HIF1α were reduced upon UBE2Q2 knockdown (Fig. S4a). WB revealed HIF1α presence in Huh-7 and LM3 cells under normoxic conditions, further increased with UBE2Q2 overexpression. Correlated with HIF1α, proteins such as VEGFA, LDHA, and GLUT1 were upregulated in the overexpression context (Fig. 5a). Even under simulated hypoxia using cobalt chloride, UBE2Q2 overexpression continued to promote HIF1α expression (Fig. 5a). Besides, the expression level of UBE2Q2 did not affect the protein levels of VHL and HIF2α (Fig. 5a). Further investigation revealed increased transcription levels of HIF1α and associated genes in UBE2Q2-augmented cells, with unchanged HIF1β, HIF2α and MYC levels (Fig. S4b). Concurrent silencing of UBE2Q2 and forced overexpression of HIF1α, confirmed by WB (Fig. 5b), suggested that HIF1α overexpression could mitigate the reduced cellular proliferation caused by UBE2Q2 knockdown, as evidenced by CCK-8 and colony assays (Fig. 5c, Fig. S4c). Glucose uptake, lactate secretion, ECAR and OCR assays indicated HIF1α could recover glycolytic and mitochondrial respiration capabilities impaired by UBE2Q2 knockdown (Fig. S4d-Fig. S4h). Subcutaneous tumors demonstrated UBE2Q2 overexpression fostered tumor growth, an effect that was abrogated by the HIF1α inhibitor PX-478 (Fig. 5d and f). IHC confirmed the increased expression of HIF1α and its target proteins with UBE2Q2 overexpression, which was inhibited by PX-478, indicating UBE2Q2 may promote HCC glycolysis and tumorigenesis via HIF1α regulation. The IHC staining of CD31 indicated that up-regulated HIF1α promoted the infiltration of endothelial cells in tumor tissue (Fig. 5g, Fig. S4i).

Considering UBE2Q2's role as a potential ubiquitin-conjugating enzyme, we preliminarily suspected an influence on HIF1α degradation. Nonetheless, UBE2Q2's overexpression still elevated HIF1α under cobalt chloride culture, excluding an effect on HIF1α proline hydroxylation and VHL-mediated degradation (Fig. 5a line1), and upon treatment with the protein synthesis inhibitor CHX, HIF1α's stability was unaffected (Fig. 6a). This led us to rule out UBE2Q2's impact on HIF1α protein degradation. TCGA RNA-seq data supported a strong correlation between UBE2Q2 and HIF1α-associated genes (Fig. S5a). Therefore, it's posited that UBE2Q2 bolsters HCC glycolysis predominantly by amplifying HIF1α transcription.

3.5 UBE2Q2 enhances the transcription level of HIF1α through NF-κB pathway

Current literature indicates that multiple signaling cascades, including WNT, MAPK, PI3K/AKT/mTOR, and NF-κB, can modulate the transcriptional activity of HIF1α [12–16]. WB analysis revealed that UBE2Q2 overexpression increased the levels of phosphorylated p65 (p-p65), whereas β-catenin, ERK1/2, and Ras remained unchanged (Fig. 6b). Pharmacological blockade of specific pathways using corynoxeine, rapamycin, LY294002, and (-)-DHMEQ to inhibit ERK1/2, mTOR, PI3K, and NF-κB respectively, demonstrated that NF-κB inhibition markedly prevented the UBE2Q2-mediated upregulation of HIF1α (Fig. 6c). This led to an investigation into the NF-κB pathway activation correlated with UBE2Q2 overexpression and subsequent HIF1α transcription elevation. Further confirmation came from observing increased levels of p-p65, IκBα, and p-IκBα, indicating UBE2Q2-mediated canonical NF-κB pathway activation (Fig. 6d). Nuclear-cytoplasmic fractionation followed by Western blot suggested that UBE2Q2 overexpression fostered the nuclear localization of p-p65 and HIF1α, effects attenuated by (-)-DHMEQ (Fig. 6e). Additionally, knockdown p65 by shRNA in Huh-7 cells overexpressed UBE2Q2 significantly inhibited the transcription and protein expression of HIF1α (Fig. 6f and g). RNA sequencing analyses reinforced a strong correlation between UBE2Q2 and downstream NF-κB pathway-related genes (Fig. S5b). Consequently, UBE2Q2 appears to activate the NF-κB pathway, enhancing HIF1α transcription.

3.6 UBE2Q2 binds cIAP1 and promotes K63 ubiquitination of RIP1 to activate NF-κB pathway

To elucidate the mechanism through which UBE2Q2 activates the NF-κB pathway in HCC cells, endogenous co-immunoprecipitation (Co-IP) using an anti-UBE2Q2 antibody and mass spectrometry were employed to pinpoint interacting proteins of UBE2Q2, complemented by searches in the National Center for Biotechnology Information (NCBI) database as a cross-reference [24]. Our focus narrowed to TNF receptor-associated factor 2 (TRAF2) and baculoviral IAP repeat-containing 2 (cIAP1), both ubiquitin ligases known for forming a complex where cIAP1/2-mediated ubiquitin chains are transferred to receptor-interacting serine/threonine kinase 1 (RIP1), subsequently facilitating the activation of the NF-κB pathway (Fig. 7a) [25]. UBE2Q2 was found to bind with cIAP1 in HCC cells (Fig. 7b). Building on prior research indicating cIAP1's role in catalyzing K11, K48, and K63 polyubiquitination of RIP1 [26], and considering UBE2Q2 as a potential ubiquitin-conjugating enzyme, we posited that UBE2Q2 might alter RIP1's

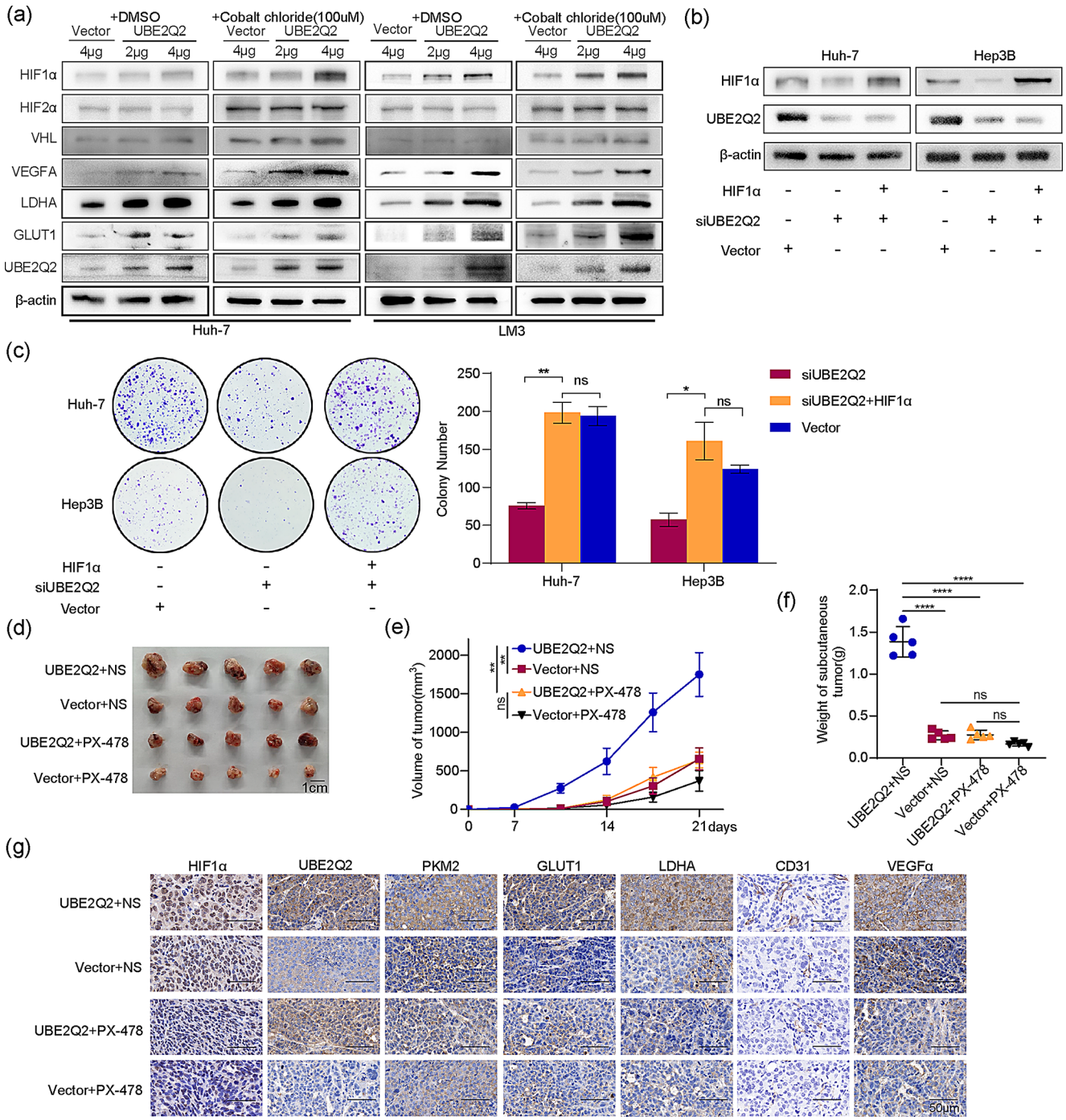

Fig. 5 UBE2Q2 promotes HCC glycolysis by enhancing the expression of HIF1α. (**a**) WB detection on HIF1α and HIF1α-related proteins with transfection of UBE2Q2 and empty vector plasmids in Huh-7 and LM3. (**b**) WB detection on HIF1α and UBE2Q2 proteins with transfection of siUBE2Q2 and HIF1α plasmids in Huh-7 and Hep3B. (**c**) Colony assay with transfection of siUBE2Q2 and HIF1α plasmids in Huh-7 and Hep3B. (**d**) Subcutaneous tumors constructed by Huh-7 UBE2Q2 cells or Huh-7 vector cells and treated with PX-478 or normal saline. (**e**) The growth curve of subcutaneous tumors treated with PX-478 or normal saline. (**f**) The weight of subcutaneous tumors treated with PX-478 or normal saline. (**g**) Representative IHC staining images of UBE2Q2, HIF1α and HIF1α-related proteins from subcutaneous tumors. Data are presented as the mean ± SD. * $p<0.05$, ** $p<0.01$, **** $p<0.0001$. NS, normal saline; ns, no significant difference

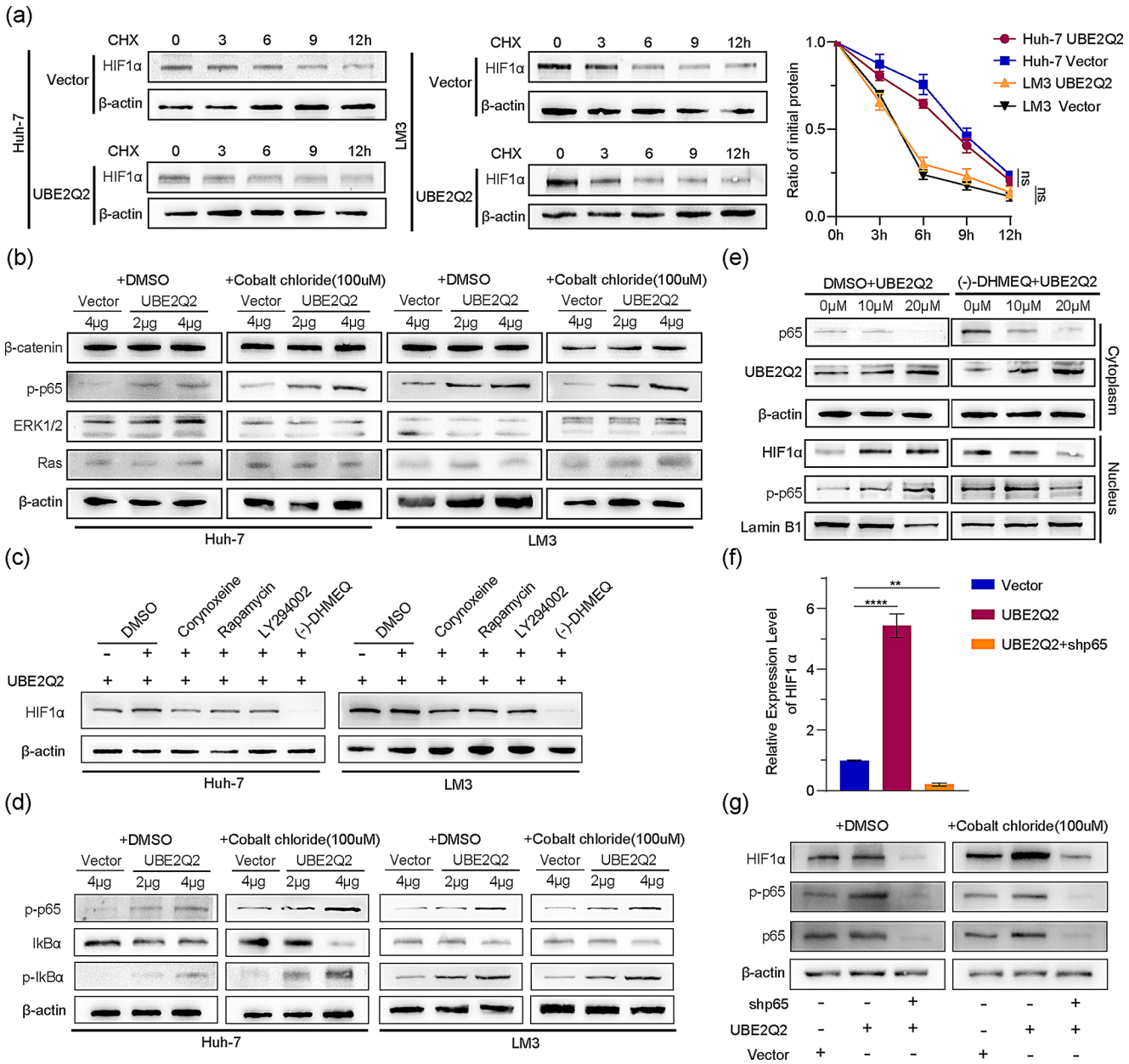

Fig. 6 UBE2Q2 enhances the transcription of HIF1α through activating NF-κB pathway. (**a**) The protein degradation rate of HIF1α is measured by WB with the treatment of CHX in Huh-7 and LM3. (**b**) WB detection on β-catenin, p-p65, ERK1/2 and Ras proteins with transfection of UBE2Q2 and empty vector plasmids in Huh-7 and LM3. (**c**) The expression of HIF1α from Huh-7 and LM3 treated with different pathway inhibitors are detected by WB. (**d**) WB detection on NF-κB pathway with transfection of UBE2Q2 or empty vector plasmids in Huh-7 and LM3. (**e**) The nucleus location of HIF1α and p-p65 are detected by nucleocytoplasmic separation WB in Huh-7 with transfection of UBE2Q2 plasmids under the treatment of (-)-DHMEQ. (**f**) The transcription level of HIF1α is measured by qPCR in Huh-7 cells transfected with UBE2Q2 plasmid and shp65. (**g**) The protein level of HIF1α is measured by WB in Huh-7 cells transfected with UBE2Q2 plasmid and shp65 under the treatment of DMSO or Cobalt chloride. Data are presented as the mean±SD. ** $p<0.01$, **** $p<0.0001$. CHX, chlorhexidine; ns, no significant difference

ubiquitination. Ubiquitination assays confirmed UBE2Q2 overexpression promoted RIP1 ubiquitination (Fig. 7c). Enhanced RIP1 ubiquitination was observed specifically with transfection of ubiquitin plasmid containing all mutant lysine sites (lysine mutates to arginine) except from wild-type lysine 63 (HA-Ub(K63)), while transfection of ubiquitin plasmid containing all mutant lysine sites except from wild-type lysine 11 (HA-Ub(K11)) or transfection of ubiquitin plasmid containing all mutant lysine sites except from wild-type lysine 48 (HA-Ub(K48)) had no such effect (Fig. 7d). Immunoblotting with a K63-linkage-specific polyubiquitin antibody corroborated increased K63-linked ubiquitination

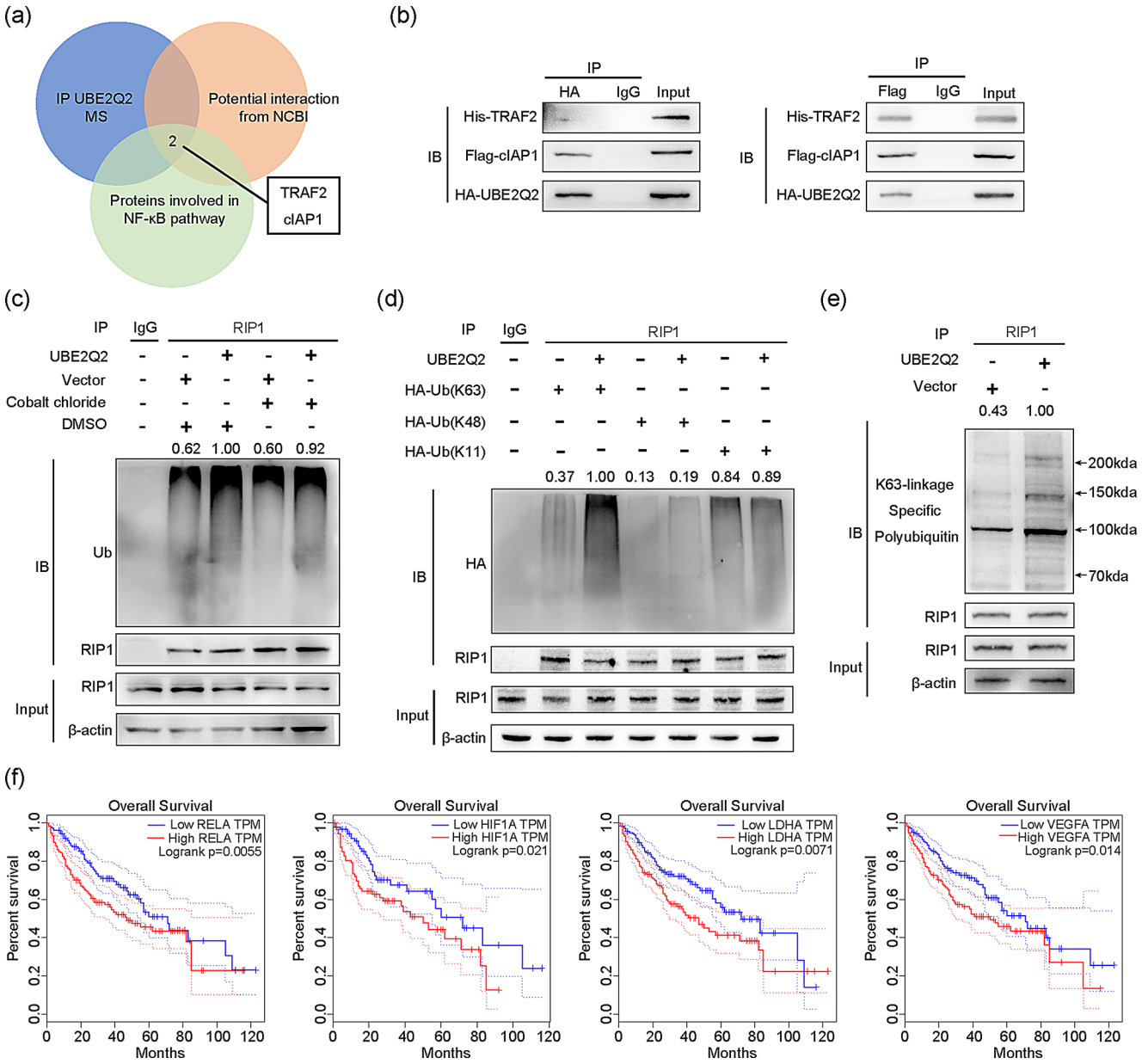

Fig. 7 UBE2Q2 binds cIAP1 and promotes K63 ubiquitination of RIP1. (**a**) The mass spectrometry results of endogenous Co-IP experiments (IP: anti-UBE2Q2), potential interaction protein list from NCBI and proteins involved in NF-κB pathway are intersected to demonstrate that UBE2Q2 might combine with TRAF2 and cIAP1. (**b**) Exogenous Co-IP and immunoblot detection from Huh-7 co-transfected by His-TRAF2, Flag-cIAP1 and HA-UBE2Q2 plasmids. (**c**) Ubiquitination assay detects RIP1 ubiquitination in Huh-7 cells transfected with UBE2Q2 or empty vector plasmids. (**d**) Ubiquitination assay detects RIP1 ubiquitination in Huh-7 cells co-transfected with UBE2Q2 and HA-Ub(K11) or HA-Ub(K48), HA-Ub(K63) plasmids. (**e**) Ubiquitination assay detects RIP1 ubiquitination in Huh-7 cells using K63-linkage specific polyubiquitin antibody. (**f**) Kaplan-Meier OS curve of RELA, HIF1α, LDHA and VEGFA from GEPIA website. (Data from TCGA databases. Median expression is used for the cutoff of groups. Log-rank test is used to calculate P value)

of RIP1 upon UBE2Q2 overexpression (Fig. 7e). Analysis of Kaplan-Meier curves from the TCGA database linked the UBE2Q2/NF-κB/HIF1α axis to poor HCC patient prognosis (Fig. 7f), suggesting that targeting this axis could be pivotal in improving survival outcomes.

4 Discussion

Primary liver cancer ranks as one of the leading causes of cancer-related mortality globally. The high fatality rate stems chiefly from challenges in early detection, high postoperative recurrence, and limited treatment effectiveness [27]. Malignant tumors commonly exhibit aerobic

glycolysis, characterized by escalated glucose consumption and lactate production, bolstering tumor cell proliferation [28]. Glycolytic inhibition has been implicated not only in suppressing tumorigenesis and angiogenesis but also in enhancing immune cell function [29, 30].

Our investigation revealed overexpression of UBE2Q2, a putative ubiquitin-conjugating enzyme, in hepatocellular carcinoma (HCC), correlating with poorer patient prognosis. UBE2Q2 appears to drive HCC progression both in vitro and in vivo by facilitating HIF1α transcription. The mechanistic pathway entails UBE2Q2 binding with cIAP1 to trigger K63 ubiquitination of RIP1, thereby activating the NF-κB pathway, which in turn augments HIF1α transcription.

Previous research has linked abnormal UBE2Q2 overexpression to malignancies such as hypopharyngeal cancer, pediatric acute lymphoblastic leukemia, and breast cancer [20, 21, 31]. HeLa cells exhibit increased chemotherapeutic sensitivity upon UBE2Q2 knockdown without altering cell cycle distribution [19]. This study, however, demonstrated that UBE2Q2 knockdown in HCC cells leads to G2/M phase arrest and is associated with G2/M checkpoint and DNA damage repair pathways, as per gene set enrichment analysis of TCGA data. Our findings also suggest UBE2Q2's involvement in glycolytic enhancement by upregulating key enzymes like PKM2, PFKL, and HIF1α. Multiple studies reveal a link between apoptosis, G2/M phase arrest, and the glycolytic activity of HIF1α, LDHA in tumor cells [32–35], underscoring UBE2Q2's oncogenic role in HCC.

The canonical NF-κB pathway is essential for inflammatory responses, cellular proliferation, differentiation, and survival [36]. Persistent activation of this pathway can, however, drive tumor progression as seen in HBV-induced HCC [37]. Moreover, NF-κB has been implicated in metabolic reprogramming towards glycolysis and increasing HIF1α transcription [38, 39]. Our study corroborates UBE2Q2's role in promoting HCC glycolysis and tumor growth through HIF1α transcriptional regulation, with (-)-DHMEQ inhibition indicating UBE2Q2's possible mediation via the NF-κB pathway. Yet, the absence of numerous differentially expressed NF-κB proteins in the proteomic assay suggests UBE2Q2's involvement might extend beyond direct NF-κB activation.

The NF-κB pathway and Warburg effect have deep interplay. For instance, the activation of the NF-kB pathway can lead to the increased expression of key enzymes involved in glycolysis, driving the Warburg effect [40]. Pro-inflammatory cytokines released as a result of NF-kB activation can also indirectly support the Warburg effect by fostering a microenvironment conducive to metabolic alterations [41]. In the same time, the metabolic reprogramming in cancer cells results in the accumulation of reactive oxygen species and other byproducts, which can further activate the NF-kB pathway, creating a positive feedback loop [42]. Our study substantiated their crucial molecular cross-talk is pathogenic in HCC.

The exact role of UBE2Q2 within the ubiquitin system remains elusive, with prior research identifying its interaction with cIAP1/2's RING domain [24]. Our work not only substantiates cIAP1 as an interacting protein but also presents evidence of UBE2Q2-engaged K63 ubiquitination of RIP1, marking the first revelation of UBE2Q2 modifying protein ubiquitination. This K63 ubiquitination alteration suggests UBE2Q2's activity within ubiquitin conjugation and its participation in NF-κB pathway activation.

In sum, UBE2Q2 propels HCC tumorigenesis and glycolysis by activating the NF-κB/HIF1α pathway, offering novel therapeutic avenues for tumor treatment.

Supplementary Information The online version contains supplementary material available at https://doi.org/10.1007/s13402-025-01037-w.

Acknowledgements We would like to acknowledge teachers from the Scientific Research Center of Zhongnan Hospital of Wuhan University for their help in this study.

Author contributions F.Y.Y., L.X.W. and R.Y.C. designed the experiments. L.X.W., R.Y.C., X.C., Y.Y., Y.Y.L., P.X., H.Z., H.Y.G. and M.X.L. performed the experiments. L.X.W., R.Y.C. and J.W.M. analyzed the data. L.X.W. and R.Y.C. wrote the manuscript. Z.W.H., F.Y.Y. and J.W.M. supervised the study. All authors reviewed the manuscript.

Funding This research is supported by Research Fund of the Health Commission of Hubei Province (WJ2021M255), Cancer research and translational platform project of Zhongnan Hospital of Wuhan University (ZLYNXM202004) and Translational medicine and interdisciplinary research joint fund project of Zhongnan Hospital of Wuhan University (ZNJC201918).

Data availability The data of this study are included in this article and its online supplementary material files. Mass spectrum results of co-immunoprecipitation using UBE2Q2 antibody were uploaded to iProX website (https://www.iprox.cn/page/, Project ID: IPX0010083000). Please contact the corresponding author if any further information is required.

Declarations

Ethical approval The collection of tissue samples and information from HCC patients was approved by the Ethics Committee of Zhongnan Hospital, approval number KELUN2018013. All patients signed the informed consent in accordance with the Declaration of Helsinki. The animal procedures were reviewed and approved by the Animal Ethics Committee of Zhongnan Hospital of Wuhan University.

Competing interests The authors declare no competing interests.

References

1. H. Sung, J. Ferlay, R.L. Siegel, M. Laversanne, I. Soerjomataram, A. Jemal et al., Global Cancer statistics 2020: GLOBOCAN estimates of incidence and Mortality Worldwide for 36 cancers in 185 countries. CA Cancer J. Clin. **71**(3), 209–249 (2021)
2. M. Seehawer, L. D'Artista, L. Zender, The worst from both worlds: cHCC-ICC. Cancer Cell. **35**(6), 823–824 (2019)
3. A. Villanueva, Hepatocellular Carcinoma, N Engl. J. Med. **380**(15), 1450–1462 (2019)
4. E. Chakraborty, D. Sarkar, Emerging therapies for Hepatocellular Carcinoma (HCC). Cancers (Basel). **14**(11) (2022)
5. O. Warburg, On the origin of cancer cells. Science. **123**(3191), 309–314 (1956)
6. Q.T. Chen, Z.Y. Zhang, Q.L. Huang, H.Z. Chen, W.B. Hong, T. Lin et al., HK1 from hepatic stellate cell-derived extracellular vesicles promotes progression of hepatocellular carcinoma. Nat. Metab. **4**(10), 1306–1321 (2022)
7. Y. Niu, Z. Lin, A. Wan, L. Sun, S. Yan, H. Liang et al., Loss-of-function genetic screening identifies aldolase A as an essential driver for Liver Cancer Cell Growth under Hypoxia. Hepatology. **74**(3), 1461–1479 (2021)
8. L. Zhao, M. Kang, X. Liu, Z. Wang, Y. Wang, H. Chen et al., UBR7 inhibits HCC tumorigenesis by targeting Keap1/Nrf2/Bach1/HK2 and glycolysis. J. Exp. Clin. Cancer Res. **41**(1), 330 (2022)
9. F. Yang, L. Hilakivi-Clarke, A. Shaha, Y. Wang, X. Wang, Y. Deng et al., Metabolic reprogramming and its clinical implication for liver cancer. Hepatology. **78**(5), 1602–1624 (2023)
10. Q. Wu, L. You, E. Nepovimova, Z. Heger, W. Wu, K. Kuca et al., Hypoxia-inducible factors: master regulators of hypoxic tumor immune escape. J. Hematol. Oncol. **15**(1), 77 (2022)
11. G.N. Masoud, W. Li, HIF-1alpha pathway: role, regulation and intervention for cancer therapy. Acta Pharm. Sin B **5**(5), 378–389 (2015)
12. S. Dong, S. Liang, Z. Cheng, X. Zhang, L. Luo, L. Li et al., ROS/PI3K/Akt and Wnt/beta-catenin signalings activate HIF-1alpha-induced metabolic reprogramming to impart 5-fluorouracil resistance in colorectal cancer. J. Exp. Clin. Cancer Res. **41**(1), 15 (2022)
13. K.C. Allan, L.R. Hu, M.A. Scavuzzo, A.R. Morton, A.S. Gevorgyan, E.F. Cohn et al., Non-canonical targets of HIF1a impair oligodendrocyte progenitor cell function. Cell. Stem Cell. **28**(2), 257–272 (2021). e11
14. T. Pan, S. Sun, Y. Chen, R. Tian, E. Chen, R. Tan et al., Immune effects of PI3K/Akt/HIF-1alpha-regulated glycolysis in polymorphonuclear neutrophils during sepsis. Crit. Care. **26**(1), 29 (2022)
15. Z.L. Li, J.L. Ji, Y. Wen, J.Y. Cao, N. Kharbuja, W.J. Ni et al., HIF-1alpha is transcriptionally regulated by NF-kappaB in acute kidney injury. Am. J. Physiol. Ren. Physiol. **321**(2), F225–F35 (2021)
16. J. Li, J. Shen, Z. Wang, H. Xu, Q. Wang, S. Chai et al., ELTD1 facilitates glioma proliferation, migration and invasion by activating JAK/STAT3/HIF-1alpha signaling axis. Sci. Rep. **9**(1), 13904 (2019)
17. P.H. Maxwell, M.S. Wiesener, G.W. Chang, S.C. Clifford, E.C. Vaux, M.E. Cockman et al., The tumour suppressor protein VHL targets hypoxia-inducible factors for oxygen-dependent proteolysis. Nature. **399**(6733), 271–275 (1999)
18. S. Han, R. Wang, Y. Zhang, X. Li, Y. Gan, F. Gao et al., The role of ubiquitination and deubiquitination in tumor invasion and metastasis. Int. J. Biol. Sci. **18**(6), 2292–2303 (2022)
19. S. Banerjee, W.S. Brooks, D.F. Crawford, Inactivation of the ubiquitin conjugating enzyme UBE2Q2 causes a prophase arrest and enhanced apoptosis in response to microtubule inhibiting agents. Oncogene. **26**(45), 6509–6517 (2007)
20. A. Seghatoleslam, A. Monabati, F. Bozorg-Ghalati, M. Nikseresht, M.R. Bordbar, M. Rahvar et al., Expression of UBE2Q2, a putative member of the ubiquitin-conjugating enzyme family in pediatric acute lymphoblastic leukemia. Arch. Iran. Med. **15**(6), 352–355 (2012)
21. A. Cromer, A. Carles, R. Millon, G. Ganguli, F. Chalmel, F. Lemaire et al., Identification of genes associated with tumorigenesis and metastatic potential of hypopharyngeal cancer by microarray analysis. Oncogene. **23**(14), 2484–2498 (2004)
22. J. Feng, J. Li, L. Wu, Q. Yu, J. Ji, J. Wu et al., Emerging roles and the regulation of aerobic glycolysis in hepatocellular carcinoma. J. Exp. Clin. Cancer Res. **39**(1), 126 (2020)
23. T. Kashihara, R. Mukai, S.I. Oka, P. Zhai, Y. Nakada, Z. Yang et al., YAP mediates compensatory cardiac hypertrophy through aerobic glycolysis in response to pressure overload. J. Clin. Invest. **132**(6) (2022)
24. J.N. Dynek, T. Goncharov, E.C. Dueber, A.V. Fedorova, A. Izrael-Tomasevic, L. Phu et al., c-IAP1 and UbcH5 promote K11-linked polyubiquitination of RIP1 in TNF signalling. EMBO J. **29**(24), 4198–4209 (2010)
25. M. Darding, P. Meier, IAPs: guardians of RIPK1. Cell. Death Differ. **19**(1), 58–66 (2012)
26. A. Witt, D. Vucic, Diverse ubiquitin linkages regulate RIP kinases-mediated inflammatory and cell death signaling. Cell. Death Differ. **24**(7), 1160–1171 (2017)
27. J.M. Willatt, I.R. Francis, P.M. Novelli, R. Vellody, A. Pandya, V.N. Krishnamurthy, Interventional therapies for hepatocellular carcinoma. Cancer Imaging. **12**, 79–88 (2012)
28. M.G. Vander Heiden, L.C. Cantley, C.B. Thompson, Understanding the Warburg effect: the metabolic requirements of cell proliferation. Science. **324**(5930), 1029–1033 (2009)
29. S. Ganapathy-Kanniappan, J.F. Geschwind, Tumor glycolysis as a target for cancer therapy: progress and prospects. Mol. Cancer. **12**, 152 (2013)
30. C. Chelakkot, V.S. Chelakkot, Y. Shin, K. Song, Modulating glycolysis to improve cancer therapy. Int. J. Mol. Sci. **24**(3) (2023)
31. M. Nikseresht, A. Seghatoleslam, A. Monabati, A. Talei, F.B. Ghalati, A.A. Owji, Overexpression of the novel human gene, UBE2Q2, in breast cancer. Cancer Genet. Cytogenet. **197**(2), 101–106 (2010)
32. S.M. Manohar, A.A. Padgaonkar, A. Jalota-Badhwar, S.V. Rao, K.S. Joshi, Cyclin-dependent kinase inhibitor, P276-00, inhibits HIF-1alpha and induces G2/M arrest under hypoxia in prostate cancer cells. Prostate Cancer Prostatic Dis. **15**(1), 15–27 (2012)
33. X. Zhai, Y. Yang, J. Wan, R. Zhu, Y. Wu, Inhibition of LDH-A by oxamate induces G2/M arrest, apoptosis and increases radiosensitivity in nasopharyngeal carcinoma cells. Oncol. Rep. **30**(6), 2983–2991 (2013)
34. M. Achison, T.R. Hupp, Hypoxia attenuates the p53 response to cellular damage. Oncogene. **22**(22), 3431–3440 (2003)

35. S. Ohba, Y. Tang, T.A. Johannessen, J. Mukherjee, PKM2 interacts with the Cdk1-CyclinB complex to facilitate cell cycle progression in Gliomas. Front. Oncol. **12**, 844861 (2022)
36. H. Yu, L. Lin, Z. Zhang, H. Zhang, H. Hu, Targeting NF-kappaB pathway for the therapy of diseases: mechanism and clinical study. Signal. Transduct. Target. Ther. **5**(1), 209 (2020)
37. M. Karin, Nuclear factor-kappab in cancer development and progression. Nature. **441**(7092), 431–436 (2006)
38. L. Liang, Y. Zhu, J. Li, J. Zeng, L. Wu, ALKBH5-mediated m6A modification of circCCDC134 facilitates cervical cancer metastasis by enhancing HIF1A transcription. J. Exp. Clin. Cancer Res. **41**(1), 261 (2022)
39. M. Arra, G. Swarnkar, K. Ke, J.E. Otero, J. Ying, X. Duan et al., LDHA-mediated ROS generation in chondrocytes is a potential therapeutic target for osteoarthritis. Nat. Commun. **11**(1), 3427 (2020)
40. X. Liu, Z. Gao, X. Wang, Y. Shen, Parthenolide targets NF-kappaB (P50) to inhibit HIF-1alpha-mediated metabolic reprogramming of HCC. Aging (Albany NY). **14**(20), 8346–8356 (2022)
41. R. Jiang, S. Luo, M. Zhang, W. Wang, S. Zhuo, Y. Wu et al., Ginsenoside Rh4 inhibits inflammation-related hepatocellular carcinoma progression by targeting HDAC4/IL-6/STAT3 signaling. Mol. Genet. Genomics. **298**(6), 1479–1492 (2023)
42. F. Yin, Y. Zhang, X. Zhang, M. Zhang, Z. Zhang, Y. Yin et al., The ROS/NF-kappaB/HK2 axis is involved in the arsenic-induced Warburg effect in human L-02 hepatocytes. Int. J. Environ. Health Res. **34**(1), 150–165 (2024)